Natural Convection and Columnar-to-Equiaxed Transition Prediction in a Front-Tracking Model of Alloy Solidification

J. BANASZEK, S. MCFADDEN, D.J. BROWNE, L. STURZ, and G. ZIMMERMANN

A meso-scale front-tracking model (FTM) of nonequilibrium binary alloy dendritic solidification has been extended to incorporate Kurz, Giovanola, and Trivedi (KGT) dendrite kinetics and a Scheil solidification path. Model validation *via* comparison with thermocouple measurements from a solidification experiment, in which natural convection is limited by design, is presented. *Via* solution of the flow field due to natural thermal buoyancy, it is shown that resultant liquid-phase convection creates conditions in which equiaxed solidification is favored. Comparison with simulations in which casting solidification is diffusion controlled show that natural convection has greatest effect at intermediate times, but that at early and late stages of columnar solidification, the differences are relatively small. It is, however, during the time of greatest divergence between the simulations that the authors' predictive index for equiaxed zone formation is enhanced most by convection. Finally, the columnar-to-equiaxed transition is directly simulated, in directional solidification controlled by diffusion.

DOI: 10.1007/s11661-007-9140-7

I. INTRODUCTION

RESEARCH within the last decade has led to new models in which solidification micro- and macrostructure is computed. Significant early progress was made in the combination of cellular automata (CA) techniques to model multiple grain growth with finite element analysis (FEA) to solve the global transport equations.[1] It is the goal of much recent research to separately model solidification of columnar and equiaxed grains and thereby to predict the columnar-to-equiaxed transition (CET) in solidifying alloys. At the microscopic length scale, both the phase field method[2] and the front-tracking technique[3] have been used successfully to model dendritic growth in a few crystals. Significant advances have been made in predicting CET, using CA[4] and phase field[5] methods, albeit for unidirectional solidification and in thermal fields that are fixed *a priori*. Another recent model uses a volume-averaging approach[6] in which columnar and equiaxed grains grow with very simplified morphologies, and direct numerical simulation of growth of equiaxed grains is not carried out.

The current work relates to models of the evolution of macrostructure, *i.e.*, columnar and equiaxed grains. A front-tracking formulation is applied, not at the length scale of the dendrite,[3] but at that of the grain.[7] The meso-scale model has some similarities to that developed by Flood and Hunt[8] but is not restricted to one dimension. Here, an envelope of solid is considered, enclosing either a columnar front or an equiaxed grain, and the authors use this to develop a model to predict the CET in castings in the presence of natural thermal convection. This article presents (a) experimental validation of the core model; (b) simulation of convection in the melt and the columnar mushy zone, which is directly coupled to the front-tracking formulation; and (c) a study of the front-tracking predictions of impingement of equiaxed grains with the columnar front to form a columnar-to-equiaxed transition (CET).

II. THE FRONT-TRACKING MODEL

Details of the computational approach used in the direct front tracking of undercooled solidification boundaries are available elsewhere.[7] Only a brief summary is presented here. Following nucleation at an appropriate temperature, the model[7] follows the growth of columnar or equiaxed solid *via* the employment of representative computational markers, at a speed set by dendrite kinetics, over the fixed-grid domain into undercooled liquid.

To account, in theoretical models, for nonequilibrium solutal undercooling, the growth velocity v_t is defined as a function of local undercooling, $\Delta T = T_L - T_t$, determined from the current temperature field, where T_L is the alloy equilibrium *liquidus* temperature and T_t is the dendrite tip temperature.[9] In References 7 and 10, the parabolic relationship, developed by Burden and Hunt,[11] between tip velocity v_t and the local undercooling ΔT was used, which is valid for constrained growth

J. BANASZEK, Dean, is with the Warsaw University of Technology, 00-665, Warsaw, Poland. S. McFADDEN, Postdoctoral Researcher, and D.J. BROWNE, Senior Lecturer, are with University College Dublin, Belfield Dublin 4, Ireland. Contact e-mail: david.browne@ucd.ie L. STURZ, Research Scientist, and G. ZIMMERMANN, Senior Scientist, are with ACCESS e.V, D-52072, Aachen, Germany.

This article is based on a presentation made in the symposium entitled "Solidification Modeling and Microstructure Formation: in Honor of Prof. John Hunt," which occurred March 13–15, 2006 during the TMS Spring Meeting in San Antonio, Texas, under the auspices of the TMS Materials Processing and Manufacturing Division, Solidification Committee.

Article published online June 6, 2007.

of columnar dendrites at relatively high dendrite tip velocity and low thermal gradients. In this article, the widely used model of Kurz, Giovanola, and Trivedi,[12] known as the KGT model, is employed to describe dendrite tip kinetics, and a polynomial approximation to the KGT model[13,14] is adopted, where

$$v_t = K_1(\Delta T)^2 + K_2(\Delta T)^3 \qquad [1]$$

with K_1 and K_2 coefficients specific to the alloy composition.

Here, the volume averaged energy conservation equation, valid in all regions developing in a mold during alloy solidification, *i.e.*, in the solid, columnar mush, undercooled liquid, and superheated melt zones, is solved on the Eulerian grid. Within a small but finite control volume, V_{CV}, this equation reads

$$\int_{V_{CV}} \frac{\partial(\rho c T)}{\partial t} dV + \oint_{S_{CV}} \left(\rho f_l v_{lj} H_l - \left(k \frac{\partial T}{\partial x_j} \right) \right) n_j dS = \int_{V_{CV}} (E_a + E_t) dV \qquad [2]$$

Here, ρ, c, and k are density, specific heat, and thermal conductivity of the solid-liquid mixture

$$\left.\begin{aligned} \rho &= r_s \rho_s + (1 - r_s)\rho_l \\ k &= r_s k_s + (1 - r_s) k_l \\ c &= (1 - f_l) c_s + f_l c_l \end{aligned}\right\} \qquad [3]$$

where subscripts s and l stand for the solid and liquid phases, respectively; f_l and r_s are, respectively, the mass fraction of liquid and volumetric fraction of solid, related to the entire control volume V_{CV}; T is temperature; v_{lj} and n_j are the x_j-direction liquid velocity and the corresponding component of an outward normal vector to a control volume surface S_{CV}, respectively; t is time; and H_l is the liquid enthalpy, a sum of the sensible enthalpy of the liquid phase and the latent heat, L. Equation [2] is based on the assumptions that the solid phase when formed is stationary, restricted to columnar or consolidated equiaxed solidification, and that saturation conditions exist, *i.e.*, that no pores exist, only two phases—liquid and solid. The volume integral on the right-hand side of Eq. [2] represents the latent heat source terms: E_a due to the advance of the solidification front and E_t due to dendritic thickening behind the solidification front[7,10]

$$E_a + E_t = \frac{\rho_l L}{V_{CV}} \left(g_s \frac{\partial V_m}{\partial t} + V_m \frac{\partial g_s}{\partial t} \right) \qquad [4]$$

where

$$g_s = \frac{V_s}{V_m} = \frac{V_s}{V_{CV}} \frac{V_{CV}}{V_m} = r_s \frac{V_{CV}}{V_m} \qquad [5]$$

stands for *internal* volumetric fraction of solid, which is a ratio between the solid volume, V_s, and volume of the mush, V_m, within the control volume V_{CV}.

The assumed variation of fraction solid with temperature affects the calculation of E_a, E_t, and the solid-liquid mixture properties. Because the main objective of References 7 and 10 was to analyze the potential of the new front-tracking model (FTM), a simplified linear relationship between the solid fraction and temperature was used to avoid nonlinearity of nodal energy equations. In fact, such variation should be the result of consideration of the solidification path as defined by study of interdendritic diffusion of solute in the mushy zone. Therefore, in all further presented calculations, the Scheil model of solute diffusion is used. Another improvement in the current studies is that the alloy thermophysical properties are different in the solid and in the liquid phases. It has been shown[15] that it is reasonable to assume that columnar dendrites can be represented as a single front; thus, the method does not treat individual columnar crystals. This finding has recently been exploited[16] to develop a simplified CA model of solidification. Furthermore, calculations of the progress of the columnar dendritic front in nonequilibrium solidification enable prediction, through numerical spatial integration of the undercooled region developing ahead of the front, of the potential for the formation of the equiaxed zone.[15]

III. MODELING OF SOLIDIFICATION CONTROLLED BY DIFFUSION

In microgravity conditions or when mold cooling is arranged in such way that reduces buoyancy forces (*e.g.*, directional solidification with a chill at the bottom of the mold), thermal natural convection can be ignored and the computational problem simplifies as the convective term in Eq. [2] disappears ($v_{lj} = 0$), and there is no need to solve mass and momentum conservation equations for the solid-liquid mixture. Such a situation has been analyzed in Reference 7 and the front-tracking method has been compared with the commonly used enthalpy approach in Reference 10 for Burden and Hunt kinetics[11] and for the physically unrealistic linear relationship between the fraction solid and temperature.

Here, further development of the computer simulation model is reported where the front-tracking technique is coupled with the fully implicit control volume finite difference method (CVFDM)[17] and with a special iterative algorithm written to include in the model both the Scheil solidification path and KGT kinetics (Eq. [1]).

At each successive time-step, the following iterative strategy is applied.

(1) First, using the current solid fraction field, the energy conservation Eq. [2] is solved on a control volume grid to get a current iteration of nodal temperatures.
(2) The computed temperature field, along with the adopted law of dendrite tip growth (Eq. [1]), is used to calculate the local undercooling, the local marker velocities, their new positions, and the mush volumes and to update the fraction solid for all control volumes that are bounded or crossed by the solidification fronts

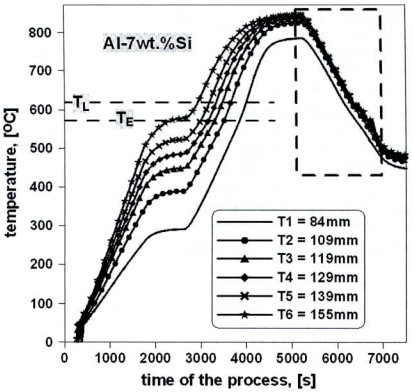

Fig. 1—Solidification experiment: temporal variation of temperature measured by six thermocouples placed at different heights of the sample.

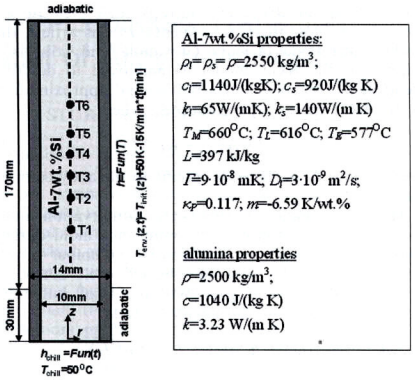

Fig. 2—Computational model of directional solidification of a cylindrical sample in the Bridgman furnace with the power down cooling strategy—geometry and boundary conditions, properties of the alloy, and the alumina crucible used.

(3) The convergence is next verified and, unless maximum differences between two consecutive iterations of temperature, two successive approximations of the fraction solid, and two consecutive updates of the mush volumes are simultaneously lower than the assumed tolerance, the source terms of Eq. [2], E_a and E_t, are recalculated and the preceding steps are repeated.

A. *Experimental Validation of the Model*

The model predictions have been compared with measurements obtained from a carefully instrumented directional solidification experiment carried out by the authors. The experiment involved solidification of a rodlike sample of binary alloy Al-7 wt pct Si under argon atmosphere in a Bridgman–Stockbarger type furnace in a thermally stable configuration with directional solidification vertically upward in the gravity field. Solutal instability is negligible because, in this case, the solute density is very similar to that of the solvent. The Bridgman furnace was equipped with a hot zone and a cold zone separated by an adiabatic zone (thermal baffle) of height 40 mm, but not used in typical mode, as will be seen. The sample material was delivered from HYDRO Aluminum GmbH (Bonn, Germany) and cast from high-purity materials. It was manufactured to fit into an alumina crucible of diameter 10 mm. The sample was partially molten within a suitable temperature gradient and solidified after thermal equilibration by extracting heat along the samples axis, the lower zone consisting of a water-cooled bath of liquid Ga-In. A "power-down" technique was applied in which the temperature of the hot zone was decreased in a controlled and constant manner, while no relative sample-furnace movement was applied.

Columnar grains of primary Al dendrites and interdendritic eutectic were formed at the beginning of the experiment, as expected at the low growth rate v_t and high-temperature gradient G. The CET occurred by lowering G within the melt ahead of the dendrite tips and increasing v_t powering down the electrical resistance heaters.

Temperature was gaged by thermocouples positioned at different axial positions in a small alumina crucible in the center of the sample. It was shown that these measurement arrangements do not visibly influence microstructural evolution, because CET occurred within 1 mm of the same position with and without temperature assessment.

The experimental results are shown in Figure 1 in terms of temporal variation in temperature measured by six thermocouples placed at different heights (see Figure 2) of the cylindrical sample of alloy. Within the first period (< 2600 seconds), the hot zone was heated from ambient to the final temperatures and the system left for some equilibration. Then, the sample was moved within the hot zone and it was thus partially molten (< 4400 seconds). After thermal equilibration, the "power-down" procedure was started at 5200 seconds, cooling at 15 °C/min until 6680 seconds.

Only the cooling/solidification part of the temperature curves (shown in Figure 1 within dashed rectangle) is the subject of comparison with the model calculations.

To numerically simulate the directional solidification of Al-7 wt pct Si alloy in a Bridgman furnace with this power-down technique, the computational model was developed with geometry and boundary conditions, as shown in Figure 2.

Conjugate heat transfer was analyzed, whereby conduction and the liquid-solid phase transformation in the sample were calculated simultaneously with conduction

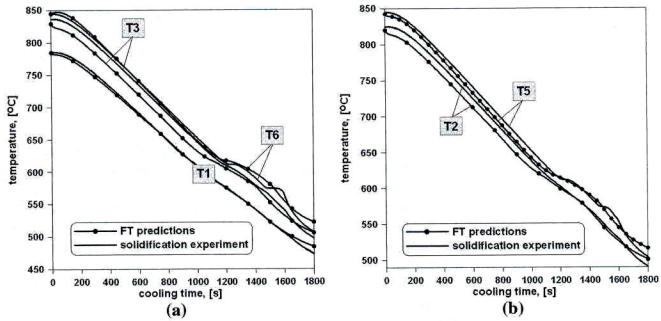

Fig. 3—Comparison of cooling curves from the solidification experiment and the FTM calculations at the selected thermocouple positions.

in the alumina crucible. Initial temperature, varying along the axis of revolution, was approximated by a piecewise linear function based on the experimental data–temperature values, T_{init}, measured by the six thermocouples at the start of the cooling process (at 5200 seconds in Figure 1).

To mimic the power-down technique, convective boundary conditions on the external curved surfaces of the ceramic crucible and on the chill/alloy surface were used with temperatures decreasing in time according to the expression shown in Figure 2.

Computations were performed on a 14×200 control-volume square grid with the fully implicit Euler scheme and $\Delta t = 0.05$ s. The Scheil solute diffusion model was employed along with KGT dendrite kinetics, Eq. [1], where $K_1 = 2.9 \cdot 10^{-6}$ m/(s K^2), and $K_2 = 1.49 \cdot 10^{-6}$ m/(s K^2).[14] Alloy and mold thermophysical properties are presented in the box in Figure 2, where T_E, Γ, D_l, and m represent the eutectic temperature, Gibbs–Thomson coefficient, solute diffusivity in the liquid phase, and slope of the liquidus in the binary phase diagram, respectively; T_M is the melting point of the pure metal and κ_p is the alloy partition coefficient.

Because surface boundary conditions were unknown quantitatively, the first *T*1 cooling curve (Figures 1 and 2) was used to calibrate the heat-transfer coefficients (htcs) on the bottom-chilled surface of the sample and on the outer curved surface of the crucible (with the baffle zone adiabatic); they were matched as corresponding functions of cooling time and temperature, respectively (Figure 2).

The model predictions of temporal changes of temperature at the six selected thermocouple locations are compared with the experiment findings in Figure 3, which shows reasonable agreement between measurements and calculations. Larger experimental solidification plateaux or recalescences are obvious in those parts of the casting that are last to solidify, probably caused by equiaxed solidification or the eutectic arrest. Deviations from the predicted curves occur here as the model is of columnar growth alone. However, as outlined in Section V, progress on overcoming this limitation is being made.

Furthermore, choosing values of htc to force agreement at *T*1 does not guarantee the same fit elsewhere. More precise information on both boundary conditions is needed if the agreement is to be more universal. For this, more extensive system temperature measurements would be needed, including those in the mold, which, with appropriate inverse models, could be used to compute the system htcs.[18]

IV. MODELING OF COLUMNAR SOLIDIFICATION WITH CONVECTION

It has long been known that buoyancy forces play an important role in the progress and morphology of alloy solidification. Due to the presence of natural convection, it is expected that local temperature gradients in the liquid (G) become lower than in the case of pure conduction, which may significantly change the temporal position of the liquidus isotherm in the mold and the shape of the mushy zone.

Computationally efficient single domain enthalpy/porous medium models have been commonly used in the calculations of multidimensional casting processes on the industrial scale, *e.g.*, References 19 and 20. However, as no direct account was taken of the kinetics of growth of solid, a picture of the microstructure could not emerge. In particular, such models cannot distinguish between the columnar mush and the undercooled liquid region ahead of dendrite tips, resulting from the non-equilibrium phenomenon of solutal undercooling. Moreover, because in the enthalpy approach the mushy zone is treated as a whole, the same porous medium model is used in both regions to account for the flow resistance there. However, it seems physically more convincing to restrict the porous medium flow model to the region of columnar structure, because only the morphology of this zone resembles a porous medium. In the undercooled liquid region, where equiaxed structure can develop, some models of slurry should rather be used.

However, to develop distinct models in these two zones, one needs to know the temporal position of the columnar dendritic front. Therefore, the front-tracking

technique was coupled to the macroscopic transport equations of mass, momentum, and energy of the solid-liquid mixture, and the preliminary results were reported in Reference 10 for the linear fraction solid–temperature relationship in the columnar mush and for Burden and Hunt kinetics.[11]

Here, an account is given of the extension of the authors' FTM, as applied to the simulation of solidification controlled by both conduction and thermal natural convection, to the use of a more recent treatment of dendrite tip kinetics (KGT model) and a realistic description of solute diffusion and microsegregation (Scheil function). In addition, a more complete analysis of the potential for the formation of an equiaxed zone ahead of the columnar front is conducted and compared to the pure thermal diffusion case.

To get the velocity field, v_l, Eq. [2] is supplemented with volume averaged mass and momentum conservation equations for the solid-liquid mixture. Assuming equal and constant densities of both phases ($\rho_s = \rho_l = \rho$, which also implies the equality of respective mass and volume fractions), a stationary solid phase, the Newtonian fluid model, and laminar Boussinesq thermal natural convection, the following equations are valid within a small but finite control volume V_{CV}:

$$\left.\begin{aligned} &\oint_{S_{CV}} v_j n_j dS = 0 \quad \text{for } i,j = 1,2,3 \\ &\int_{V_{CV}} \rho \frac{\partial v_i}{\partial t} dV + \oint_{S_{CV}} \left(\rho v_i v_j - \mu_l \frac{\partial v_i}{\partial x_j}\right) n_j dS = - \oint_{S_{CV}} p n_i dS + \\ &\beta_T g_i \rho_{\text{ref}} \int_{V_{CV}} r(T - T_{\text{ref}}) dV + \int_{V_{CV}} Q_{vi} dV \end{aligned}\right\} \quad [6]$$

where $v_j = f_l v_{lj}$ is a j component of the apparent velocity (mass averaged); $p = r_l p_l$ is the superficial pressure; and μ_l, g_i, and β_T are, respectively, dynamic viscosity of the liquid, component of the gravity vector, and thermal expansion coefficient of the liquid. The term ρ_{ref} stands for reference density at a reference temperature, T_{ref}.

The additional source term, Q_{vi}, is used to mimic Darcy's flow in the columnar dendrite mushy zone, V_m. Resolution of this two-phase region permeability requires detailed considerations of its developing morphology. In the present analysis, the commonly used Blake–Kozeny model is adopted, and

$$Q_{v_i} = -\mu_l K_0 \frac{g_s^2}{(1 - g_s)^3} v_i \quad [7]$$

where K_0 is a morphological constant.[19,20]

The general appearance of the preceding equations is an integral counterpart of those commonly used in the enthalpy/porous medium model of the mushy zone (for example, References 19 and 20), but when these equations are coupled with the front-tracking technique, the opportunity arises for more precise modeling of the momentum transport within the mushy zone. Having identified the curve joining the columnar dendrite tips at any time of the solidification process, one can restrict application of the porous medium model, Eq. [6] with Eq. [7], only to the columnar dendritic region. In the undercooled melt, some model of slurry can be adopted when equiaxed dendrite structure develops, or the source term, Eq. [7], is simply nullified in the case where nucleation and grain growth have not yet started there.

The KGT description of dendrite kinetics is based on diffusion in the liquid solute field surrounding the growing tip. A more advanced model would treat the additional effect of liquid flow on dendritic growth, *e.g.*, using kinetics as modified by Schrage[21] or Gandin *et al.*[22] Direct coupling of dendrite kinetics to both the thermal and liquid velocity field, v_l, in a convergent, iterative, and self-consistent manner would involve a significant extra model complexity and computational overhead. The authors plan to carry this out in the future and compare the results to the current ones. For now, it is assumed that the growth kinetics are not influenced by velocity field, v_l.

To calculate concurrent fluid flow and heat-transfer phenomena occurring in the superheated melt, undercooled liquid, mushy, and fully solidified regions, the CVFDM was directly coupled with the front-tracking technique on a fixed grid. The authors' computational model is based on the staggered grid approach,[17] to avoid checkerboard pressure modes, and on the power-law upwinding,[17] to eliminate nonphysical spatial oscillations of the numerical solution. To separately calculate pressure and velocity fields, the velocity and pressure correction method[23] is used. Finally, the iterative segregated solution strategy is used, where linearized directional momentum and energy equations are solved consecutively. When a fully implicit time marching scheme is used, the convective-diffusive energy equation coupled with the front-tracking technique is solved in an inner iterative loop analogous to the one described in Section III of the article.

The example of columnar dendrite solidification of Al-4 wt pct Cu in a square mold cooled from all sides by convective heat transfer (Figure 4) was used to study the effect of thermal natural convection on the development of columnar dendritic and undercooled liquid zones. The alloy properties are listed in Figure 4 and they are supplemented with $\mu = 1.3 \cdot 10^{-3}$ kg/(ms) and $\beta_T = 10^{-4}$ K^{-1}. At the start of the process, the melt was at a temperature of 700°C. It was then cooled by convective heat flux, q_b, through all external surfaces of the mold (Figure 4) with the constant ambient temperature

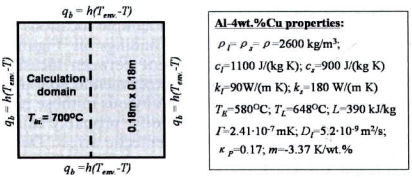

Fig. 4—Geometry, boundary conditions, and thermophysical properties for columnar solidification of Al-4 wt pct Cu.

T_{env} = 400°C and the heat-transfer coefficient h = 3 kW/(m^2 K).

Because natural convection was modeled, there was no longer fourfold symmetry (as in Reference 7), and so one half of the domain (either side of the vertical centerline) was divided into 50 × 100 staggered control volumes.

The KGT model of dendrite growth kinetics, Eq. [1], and Scheil solidification were employed, and it was assumed that no equiaxed grains formed yet in the undercooled liquid region. In the absence of equiaxed solidification in this zone, the columnar front could proceed unhindered to the center of the casting. The undercooled region was treated as completely liquid, although with temperatures lower than the equilibrium liquidus temperature.

The columnar dendritic zone was modeled as isotropic porous medium where the resistance to the flow was given by Blake–Kozeny law,[19,20] Eq. [7], with the estimated morphological constant $K_o = 4.92 \cdot 10^7$ m^{-1}.

To analyze the impact of natural thermal convection on the developing columnar dendritic and undercooled liquid zones, the predicted temporal positions of the dendrite tip curve and of the liquidus isotherm are compared in Figures 5 and 6 for solidification driven by convection vs that controlled only by conduction.

The differences in the dendrite tip curves (Figure 5), although visible, are not very substantial. Nevertheless, the local temperature gradients lowered by thermal buoyancy forces cause a faster movement of the liquidus isotherm toward the hottest central part of the mold (Figure 6). Thus, the undercooled liquid zone, confined by this isotherm and the dendrite tip curve, becomes much larger when compared with the case of pure conduction. This is particularly observed at early and intermediate times of the solidification process, where relatively strong convection currents occur (Figure 6). At later times, when a significant part of the mold is filled with the solid, the region of superheated melt is shortened, being replaced by the liquid of temperature slightly lower than the liquidus, and thermal convection becomes very weak. In consequence, all zones, i.e., the solid, columnar, and undercooled ones, resemble the corresponding zones growing during conduction-controlled solidification (Figure 6).

As mentioned, Browne[15] used the FTM of nonequilibrium columnar solidification to estimate the potential for the formation of a completely equiaxed structure developing in front of the columnar zone. The proposed equiaxed index is calculated by numerical integration of the local undercooling, ΔT, over all control volumes within which the undercooling occurred and can be treated as a metric for the relative tendency to form an equiaxed zone.[15] It was shown that low heat-transfer

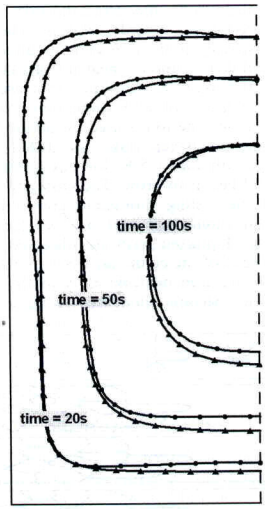

Fig. 5—Comparison of temporal positions of the columnar dendritic front during solidification of Al-4 pct wt Cu controlled by pure conduction—curves with solid triangles, and additionally by thermal natural convection—curves with solid circles.

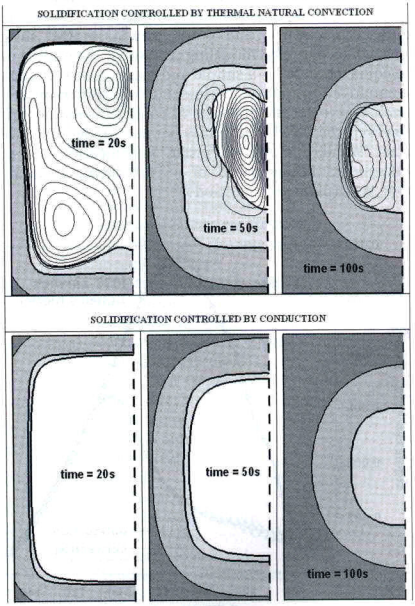

Fig. 6—Comparison of FTM predictions of evolution of the solid, liquid, columnar, and undercooled liquid zones during solidification controlled by conduction and natural convection; solid—dark gray, columnar zone—gray; undercooled liquid—light gray, and superheated melt—white.

coefficients and increasing the solute content in the alloy augmented the index, thus indicating higher potential of promotion of equiaxed solidification. Recently, it has been shown[24] that predictions based on this index concur well with Hunt[25] CET maps in (G, v_t) space.

Here, the equiaxed index is used to study the role of thermal natural convection in the development of equiaxed solidification. Figure 7 compares the index for columnar solidification of Al-4 wt pct Cu with and without natural convection in the melt intensively cooled (h = 3000 W/(m^2 K) in the square mold, Figure 4).

In both cases, the equiaxed index behaves in a similar way. At the start of solidification, it is very small, as the extent of the undercooled region ahead of the front is small (left column of Figure 6). Next, the index increases, reaching its peak at some intermediate time, but eventually starts to decrease as columnar solidification converges at the casting center and the undercooled region contracts (right column of Figure 6). However, in the case of thermal natural convection, the potential of forming an equiaxed zone is roughly 2 times higher than that calculated for pure heat diffusion, and it gains its maximum much earlier (Figure 7).

All of this confirms that natural thermal convection in interdendritic and bulk liquids alters the local undercooling and thus changes the conditions created for equiaxed nucleation and grain growth. It also shows that, while actually modeling columnar solidification, the equiaxed index is a simple and useful metric that can be employed to tailor experimental variables in order to increase or lower the potential of equiaxed solidification. However, the FTM is currently being extended to enable direct simulation of equiaxed solidification in the undercooled liquid ahead of an advancing columnar front, as explained in Section V.

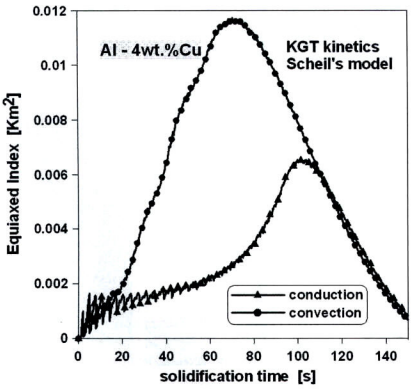

Fig. 7—Comparison of temporal changes of the equiaxed index during solidification of Al-4 wt pct Cu controlled by pure conduction—curve with solid triangles, and by thermal natural convection—curve with solid circles.

V. MODELING EQUIAXED SOLIDIFICATION AND IMPINGEMENT

Equiaxed crystals may nucleate in the undercooled liquid ahead of the advancing columnar dendrites. These equiaxed forms become dendritic and continue to grow until they impinge with neighboring dendrites. Where the grains impinge, an as-cast grain boundary is observed. If the neighboring dendrites to the equiaxed ones are columnar, then a CET is seen. Front tracking has been used to model the growth of isolated equiaxed dendrites[7] and has recently been developed to include impingement of the equiaxed dendrites[26] in a purely diffusive system. Thermal interaction between growing grains affects the tip undercooling and, consequently, the relative growth velocities between neighboring grains. Hence, thermally soft impingement occurs, that is, the approaching growth velocities gradually reduce as the grains get closer to each other. The authors have recently demonstrated[27] that thermal effects, due to evolving latent heat, dominate the interaction between neighboring growing dendritic crystals, for the majority of the growth stage between nucleation and impingement in typical castings. It is only very near impingement between growing grains, when grain boundary loci are largely finalized, that their solutal boundary layers overlap. Therefore, through direct modeling of the nucleation, growth, and impingement of equiaxed grains ahead of a columnar front, this FTM is capable[28] of directly simulating the final as-cast macrostructure and CET.

Figure 8 shows front-tracking results (purely diffusive case) at four time stages for an Al-2 pct wt Cu sample that is cooled from the left-hand-side wall of a 4 × 10 mm rectangular mold/enclosure. The computational grid spacing is 0.1 mm in both directions. The wall is held at 400 °C and the heat-transfer coefficient at the wall is 3000 W/m^2 K. All other walls are adiabatic. An initial superheat of 15 K is present. An instantaneous nucleation criterion is used: when the undercooling at the seed is sufficient (taken as 1.0 K for initiating columnar growth and 0.5 K for equiaxed), a crystal nucleates and begins to grow. The seeds are distributed throughout the casting. Columnar grains nucleate on the left-hand mold wall and are represented by a growing front. Equiaxed grains are observed to nucleate and grow ahead of the columnar front. For time t_1, the crystals that are seen nucleate early in the simulation and grow to become elongated columnar crystals

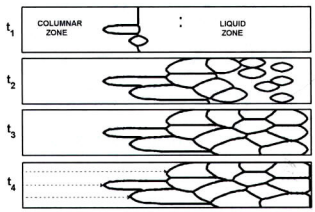

Fig. 8—Columnar and equiaxed growth of a directionally solidified Al-2 wt pct Cu.

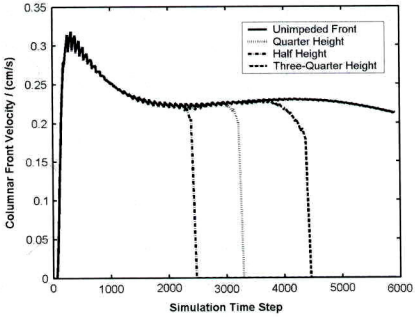

Fig. 9—Comparing the columnar front velocity at three section heights to the columnar velocity when no impingement takes place: $\Delta t = 5 \times 10^{-4}$ s.

themselves. The final result, at t_4, shows the as-cast macrostructure of the sample and the CET.

To reveal the nature of the impingement of the columnar front, the horizontal velocity of the columnar front of Figure 8 is measured over time at three heights: quarter, half, and three-quarters sample height (shown in Figure 8 at t_4). These velocities are compared to the velocity of a columnar front that is allowed to grow unimpeded to the end of the sample, that is, under the same growth conditions but with equiaxed nucleation suppressed; hence, no impingement takes place. Figure 9 shows this comparison. For the velocities of the impeded front, one observes a gradual deceleration and then an abrupt decrease to zero velocity for each measurement. The initial gradual deviation is due to the thermal interaction of the columnar front with the neighboring grains; this is thermally soft impingement. The abrupt decrease to zero occurs when the neighboring grains contact one another, and growth ceases at this point. The thermal impingement effect is more pronounced at the three-quarter height, simply because at this height the neighboring equiaxed grains nucleated earlier, grew bigger, and had a larger influence on the local temperature profile. Also, at this later time in the simulation, the thermal gradient in the liquid is lower, thus widening thermal boundary layers. The other grains that nucleated closer to the columnar front were quite small at the moment of contact and emitted only a small amount of latent heat up to that point.

VI. CONCLUSIONS

The current model was validated by comparison with a well-instrumented and carefully controlled directional solidification experiment on an Al-Si alloy. The effect of liquid flow due to thermal gradients on the undercooled region has now been computed, and it is shown that such natural thermal convection promotes equiaxed solidification, even when effects such as transport of crystalline fragments in such flow from the columnar mushy zone are neglected. Direct simulation of equiaxed solidification has been carried out, and, when done simultaneously with columnar growth simulation, the CET is computed.

Future work will entail modification of the dendrite kinetics to account for the effects of liquid flow, implementing a model of slurry to deal with the flow of the equiaxed mushy zone and direct coupling of the two flow models—that in the fixed porous columnar solid with that in the particulate two-phase equiaxed mush. Proper consideration of the effect of liquid solute gradients on natural convection will also follow.

ACKNOWLEDGMENTS

The authors are grateful to the European Space Agency for funding *via* the CETSOL (columnar-equiaxed transition in solidification processing) Microgravity Applications Promotion project (Contract No. CCN002-14313/01/NL/SH). We also thank Mr. M. Seredynski, Warsaw University of Technology, for performing some of the calculations.

NOMENCLATURE

c	specific heat
D_l	mass diffusivity in liquid
E_a	source term accounting for front advection
E_t	source term accounting for dendrite thickening
f	mass fraction
G	temperature gradient
g	internal volumetric fraction
g_i	component of gravity vector
H	specific enthalpy
h	heat-transfer coefficient
K_0	morphological constant
K_1	coefficient of KGT model
K_2	coefficient of KGT model
k	thermal conductivity
L	latent heat term, $L = (c_s - c_l)T_{\text{ref}} + L_{\text{ref}}$
L_{ref}	latent heat at reference temperature
n_i	component of outward normal
Q_v	Darcy's source term
r	volumetric fraction
S	surface
T	temperature
T_{env}	ambient temperature
T_{init}	initial temperature
T_{ref}	reference temperature
T_t	dendrite tip temperature
T_L	liquidus temperature
T_M	melting point of pure metal
t	time
V	volume
V_m	volume of columnar mush
v	apparent velocity

v_l	liquid velocity
x_i	Cartesian coordinate
β_T	thermal expansion coefficient of liquid
ΔT	temperature difference
Δt	time-step
Γ	Gibbs-Thomson coefficient
κ_p	partition coefficient
μ_l	dynamic viscosity of liquid
ρ	density
ρ_{ref}	reference density in Boussinesq model

Subscripts

CV	pertinent to control volume
i, j	Cartesian coordinate direction
l	liquid
m	pertinent to columnar mush
s	solid

REFERENCES

1. C.-A. Gandin and M. Rappaz: *Acta Metall. Mater.*, 1994, vol. 42 (7), pp. 2233–46.
2. I. Steinbach, C. Beckermann, B. Kauerauf, Q. Li, and J. Guo: *Acta Mater.*, 1999, vol. 47 (3), pp. 971–82.
3. D. Juric and G. Tryggvason: *J. Comp. Phys.*, 1996, vol. 123, pp. 127–48.
4. H.B. Dong and P.D. Lee: *Acta Mater.*, 2005, vol. 53, pp. 659–68.
5. A. Badillo and C. Beckermann: *Acta Mater.*, 2006, vol. 54, pp. 2015–26.
6. M. Wu and A. Ludwig: *Metall. Mater. Trans. A*, 2006, vol. 37A, pp. 1613–31.
7. D.J. Browne and J.D. Hunt: *Num. Heat Transfer, Part B: Fundam.*, 2004, vol. 45 (5), pp. 395–419.
8. S.C. Flood and J.D. Hunt: *J. Cryst. Growth*, 1987, vol. 82, pp. 543–51.
9. J. Banaszek, P. Furmanski, M. Rebow: *Modelling of Transport Phenomena in Cooled and Solidifying Single Component and Binary Media*, Oficyna Wydawnicza Politechniki Warszawskiej, Warsaw, 2005. ISBN 83-7207-585-9.
10. J. Banaszek and D.J. Browne: *Mater. Trans.*, 2005, vol. 46 (6), pp. 1378–87.
11. M.H. Burden and J.D. Hunt: *J. Cryst. Growth*, 1974, vol. 22, pp. 109–16.
12. W. Kurz, B. Giovanola, and R. Trivedi: *Acta Metall.*, 1986, vol. 34, pp. 823–30.
13. C.-A Gandin, C.H. Charbon, and M. Rappaz: *ISIJ Int.*, 1995, vol. 35 (6), pp. 651–57.
14. M.F. Zhu, J.M. Kim, and C.P. Hong: *ISIJ Int.*, 2001, vol. 41, pp. 992–98.
15. D.J. Browne: *ISIJ Int.*, 2005, vol. 45 (1), pp. 37–44.
16. M.A. Martorano and V.B. Biscuola: *Model. Simul. Mater. Sci. Eng.*, 2006, vol. 14, pp. 1225–43.
17. S.V. Patankar: *Numerical Heat Transfer and Fluid Flow*, Hemisphere Publishing, Washington, DC, 1980.
18. D.J. Browne and D. O'Mahoney: *Metall. Mater. Trans. A*, 2001, vol. 32 (12), pp. 3055–63.
19. W.D. Bennon and F.P. Incropera: *Num. Heat Transfer*, 1988, vol. 13, pp. 277–96.
20. C. Prakash and V.R. Voller: *Num. Heat Transfer Part B*, 1989, vol. 15, pp. 171–89.
21. D.S. Schrage: *J. Cryst. Growth*, 1999, vol. 205, pp. 410–26.
22. C.A. Gandin, G. Guillemot, B. Appolaire, and N.T. Niane: *Mater. Sci. Eng. A*, 2003, vol. 342, pp. 44–50.
23. J.P. Van Doormal and G.D. Raithby: *Num. Heat Transfer*, 1984, vol. 17, pp. 147–63.
24. M. Rebow and D.J. Browne: *Scripta Mater.*, 2006, vol. 56, pp. 481–84.
25. J.D. Hunt: *Mater. Sci. Eng.*, 1984, vol. 65, pp. 75–83.
26. S. McFadden and D.J. Browne: *Proc. Eurotherm Seminar 82 Numerical Heat Transfer 2005 (Gliwice-Cracow) 2*, A.J. Nowak, R.A. Bialecki, and G. Wecel, eds., Institute of Thermal Technology, Silesian University of Technology, Gliwice, Poland, 2005, pp. 205–14. ISBN 83-922381-2-5.
27. S. McFadden and D.J. Browne: *Scripta Mater.*, 2006, vol. 55 (10), pp. 847–50.
28. S. McFadden, D.J. Browne, and J. Banaszek: *Mater. Sci. Forum*, 2006, vol. 508, pp. 325–30.